

Quartz tuning forks resonance frequency matching for laser spectroscopy sensing

Yufei Ma^{a,*}, Yinqiu Hu^a, Shunda Qiao^a, Ziting Lang^a, Xiaonan Liu^a, Ying He^a, Vincenzo Spagnolo^b

^a National Key Laboratory of Science and Technology on Tunable Laser, Harbin Institute of Technology, Harbin 150001, China

^b PolySense Lab, Dipartimento Interateneo di Fisica, University and Politecnico of Bari, Via Amendola 173, Bari, Italy

ARTICLE INFO

Keywords:

Quartz tuning fork
Resonance frequency
Gas sensing
Quartz-enhanced photoacoustic spectroscopy
Light-induced thermoelastic spectroscopy

ABSTRACT

In this paper, we report on the performance of quartz tuning fork (QTF) based laser spectroscopy sensing employing multiple QTFs. To avoid that resonance frequency mismatching of the QTFs degrades the sensor performance, two types of resonance frequency matching method are here proposed. A system based on the coupling of two sensing modules, one based on quartz-enhanced photoacoustic spectroscopy (QEPAS) and one on light-induced thermoelastic spectroscopy (LITES) technique, was realized to validate the proposed methods. Each module employed a different QTF (QTF1 and QTF2, respectively). Operating temperature or pressure of QTF2 were regulated to match the resonance frequency of QTF1, which operated at 25.0 °C and atmospheric pressure. Without regulation, the difference between QTF1 and QTF2 resonance frequencies was 2.42 Hz and the superposition coefficient η was only 54.7%. When the temperature regulation was carried out, at a QTF2 operating temperature of 67.5 °C, an optimal η value of 95.0% was obtained. For the pressure regulation approach, if operating QTF2 at pressure of 500 Torr, η reached a value of 97.2%. The obtained results show that the proposed two methods are effective in resonance frequency matching of QTFs for gas sensing systems.

1. Introduction

Trace gases are ubiquitous, and their detection found applications in various fields such as fire alarm [1], combustion diagnosis [2], life science [3], electrical safety monitoring [4] and warning of toxic and flammable gases [5]. Therefore, the development of highly sensitive trace gas detection technique is of great significance. Owing to the advantages of high selectivity and sensitivity, non-invasive and real-time detection [6–8], optical trace gas sensing techniques are widely adopted.

In 2002, quartz-enhanced photoacoustic spectroscopy (QEPAS) was firstly proposed [9]. It consists in an indirect absorption spectroscopy technique exploiting the photoacoustic effect discovered by A.G. Bell in 1880 [10]. When a modulated laser passed through a gas sample and is selectively absorbed by the trace gas specie to be detected, acoustic waves are generated. If the laser source is focused between the prong of quartz tuning fork (QTF) the pressure waves put the QTF prongs in oscillation. These vibrations generate a charge distribution due to the piezoelectric effect [11,12], which is collected by the metal pattern

deposited on the QTF surface [13,14]. Compared with traditional optical trace gas sensing techniques such as tunable diode laser absorption spectroscopy and microphone based photoacoustic spectroscopy, QEPAS provides additional figures of merit, like compactness, laser wavelength independence and immunity to the ambient noise due to the sharp frequency response of the QTF [15–22]. A novel QTF-based gas sensing method is light-induced thermoelastic spectroscopy (LITES), which was firstly reported in 2018 [23]. After absorbed by target gas, the modulated beam laser hits the QTF surface generating a modulated localized heating. The temperature changes in QTF induced by photo-thermal conversion results in thermoelastic expansion and contraction [24–28]. These light-induced deformations, once again, generate a charge distribution that can be collected by the metal pattern, generating an electrical signal which results proportional to the portion of absorbed light from the gas sample. In LITES, QTFs can operate as a narrow-bandwidth (1 Hz), fast-response (tens of kHz), broadband, high-responsivity infrared photodetector, suitable for tunable laser-based absorption spectroscopy [29–33] for the remote and standoff trace gas detection and can be used in some harsh conditions such as

* Corresponding author.

E-mail address: mayufei@hit.edu.cn (Y. Ma).

<https://doi.org/10.1016/j.pacs.2022.100329>

Received 27 November 2021; Received in revised form 23 December 2021; Accepted 10 January 2022

Available online 11 January 2022

2213-5979/© 2022 The Author(s).

Published by Elsevier GmbH. This is an open access article under the CC BY-NC-ND license

(<http://creativecommons.org/licenses/by-nc-nd/4.0/>).

combustion field.

The performance of QTF based gas sensors can be improved by exploiting multiple QTF approaches and superimposing the signals generated from each QTF. Previously, three examples of multiple QTF-based trace gas detection methods have been proposed: 1) a multiple-quartz-enhanced photoacoustic spectroscopy (M-QEPAS) sensor which employed two QTFs to detect acoustic wave signals [34]; 2) a multiple-light-induced thermoelastic spectroscopy sensor (M-LITES) which employed two QTFs act as photodetectors [35]; 3) a coupled quartz-enhanced photoacoustic spectroscopy & light-induced thermoelastic spectroscopy (QEPAS-LITES) sensor which employed two QTFs collecting the photoacoustic wave signal and thermoelastic signal, respectively [36]. Although they demonstrated better performance with respect to single QTF setups, their improvements were limited by resonance frequency mismatching between the two QTFs employed, impeding their perfect signal superposition. For example, in M-QEPAS, only a 1.7 times signal enhancement was obtained [34], instead of the 2 times improvement expected for perfect resonance frequency matching. Resonance frequency mismatching is typical also between standard 32 KHz QTFs due to the relative uncertainty of $\pm 10 \mu\text{m}$ in the exact dimensions of the prongs and the deposited gold pattern [13].

The QTF in plane flexural resonance frequency f_0 depends on the prongs geometry, the quartz elastic properties and the surrounding gas pressure and temperature. With respect to standard operating conditions (25.0°C under vacuum), frequency shift of f_0 (Δf) can be estimated using the following equation [37,38]:

$$\frac{\Delta f}{f_0} = -\frac{\delta}{2\rho W} \left(c_1 \rho_g + \frac{c_2}{\delta} \sqrt{\frac{\eta_g \rho_g}{\pi f_0}} \right) \quad (1)$$

Where δ is the prong thickness of QTF, η_g is the dynamic viscosity of the surrounding gas, ρ is the density of quartz, W is the prong width of QTF, ρ_g is the gas density, c_1 and c_2 are geometry dependent parameters. In particular, if the surrounding pressure increases, f_0 will decrease due to gas viscosity effects and this viscosity can be in turn modified by varying the operating temperature. Thereby, f_0 can be tuned by varying the operating thermodynamic conditions (pressure and temperature), allowing to recover possible QTF resonance frequency mismatches.

In this manuscript, two types of resonance frequency matching methods are proposed. A QEPAS-LITES setup, implementing two QTFs, were adopted to validate the proposed methods. Resonance frequency matching was realized by adjusting the temperature and pressure of the QTF used for LITES. Acetylene (C_2H_2) was selected as test gas to evaluate the performance of these two techniques.

2. Experimental setup

The schematic of the experimental setup used for QTF resonance frequency matching based on temperature and pressure regulation is depicted in Fig. 1. QTF1 and QTF2 were used to detect QEPAS and LITES signal, respectively. C_2H_2 with a concentration of 2% was selected as test gas to assess the performance of these two techniques. To target the absorption line of C_2H_2 at 6534.37 cm^{-1} (1530.37 nm), a fiber-coupled, distributed feedback (DFB), continuous wave (CW) diode laser with a center wavelength of $1.53 \mu\text{m}$ and output power of 20 mW was as employed. Wavelength modulation spectroscopy (WMS) and second harmonics ($2f$) detection strategy were applied. In detail, a bias voltage and a sinusoidal voltage generated by a lock-in amplifier were fed to the tunable diode laser to vary the emission wavelength. By slowly varying the bias voltage the output wavelength of the laser was scanned across the absorption line of C_2H_2 . In our experiment, the injection current of the laser was increased from 89 mA to 129 mA and the central current was set to 109 mA at 28°C . Sinusoidal voltage was added to modulate the laser at a frequency f , so to excite the acoustic wave signal and thermoelastic signals for QEPAS and LITES, respectively. QTFs with a standard resonance frequency of 30.7 kHz were used, which have

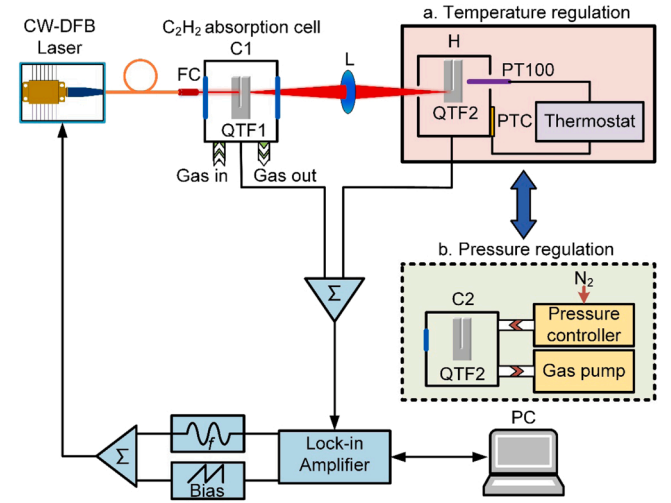


Fig. 1. Schematic diagrams of resonance frequency matching in QTFs for QEPAS-LITES based on temperature regulation and pressure regulation. Σ : adder. C1: 26 mm-long gas cell. H: steel heating cell. PTC: ceramic heating plate. PT100: temperature sensor. C2: 26 mm-long gas cell.

dimensions of 6 mm, 0.6 mm and 0.36 mm in height, prong width and thickness, respectively. QTF1 was enclosed in a 26 mm-long gas cell C1, filled with 2% $\text{C}_2\text{H}_2:\text{N}_2$, and equipped with two input and output windows made of calcium fluoride (CaF_2). The flow rate of C_2H_2 was 100 ml/min. The laser beam was collimated by a fiber collimator (FC) and pass through the QTF1 prongs without illuminating it. The laser vertical position was set 0.7 mm below the prongs top to maximize the QEPAS signal [39]. The divergent laser transmitted from C1 was focused on QTF2 by lens L with focal length of 30 mm. The focal position corresponds to the base of one of the prongs of QTF2, where the maximum strain field occurs [25,30]. The overall optical pathlength from FC to QTF2 surface was 73 mm. However, due to the design that C_2H_2 only existed in gas cell C1, an effective optical path of 20 mm was obtained for LITES approach.

For resonance frequency matching based on temperature regulation, QTF2 was installed in steel heating cell H. It had a hole at the front, allowing the laser light to hit the QTF2 and was heated by a ceramic heating plate PTC. A temperature sensor PT100 was placed close to QTF2 to monitor the temperature T_2 , which was fed back to a thermostat. T_2 was varied from 25.0°C to 70.0°C . The control accuracy for temperature regulation was 0.1°C . For resonance frequency matching based on pressure regulation, QTF2 was installed in gas cell C2, similar to C1 but filled with pure nitrogen (N_2). N_2 pressure P_2 was set by a pressure controller and a pump and was varied from 750 Torr to 475 Torr. The control accuracy for pressure regulation was 2 Torr. The flow rate of N_2 was 20 ml/min. C_2H_2 was only present in C1, where QTF1 was located, and C1 was kept at normal temperature (25.0°C) and atmospheric pressure. The regulation of temperature and pressure worked only for QTF2, to avoid any influence on physical properties of the $\text{C}_2\text{H}_2:\text{N}_2$ gas mixture. The overall optical pathlength and effective optical path remained unchanged in temperature regulation and pressure regulation. Superposition of QEPAS signal and LITES signal generated from QTF1 and QTF2, respectively, was realized by an adder. The added signal was sent to the lock-in amplifier for demodulation. Integration time of 60 ms was adopted for $2f$ demodulation with the bandwidth of 1.118 Hz. In the process of demodulation, a reference sinusoidal signal with specific frequency and phase was used to extract the signal by correlation operation. The reference frequency was an integral multiple of the modulation frequency (nf), and the phase was the one maximizing the X component. The X component for the second harmonic component ($2f$) of the system was analyzed.

3. Experimental results and discussions

3.1. QEPAS-LITES without resonance frequency matching

For realizing QEPAS-LITES setup, two QTFs were randomly selected from a set of QTF operating around 30.7 kHz to simulate a general situation. Compared with the commonly used QTF around 32 kHz, QTF with lower resonance frequency 30.7 kHz had longer accumulation time, which was beneficial to the improvement of signal amplitude. The optical excitation method was used to test the selected QTFs. The injection current of laser was kept at 109 mA to match output wavelength with the absorption peak of C₂H₂. Laser was then modulated by a sinusoidal voltage with a modulation frequency f . f was varied to retrieve the frequency response of QTF. The QTF as the detector of QEPAS module was denoted by QTF1 and another QTF as the detector of LITES module was denoted by QTF2. The characteristic parameters (resonance frequency f_0 and quality factor Q) for QTF1 (f_1 and Q_1) and QTF2 (f_2 and Q_2) were retrieved by a Lorentzian fit of the measured data, as shown in Fig. 2. For two QTFs resulted: $f_1 = 30,707.75$ Hz, $f_2 = 30,710.17$ Hz with related bandwidth $\Delta f_1 = 2.42$ Hz, $\Delta f_2 = 2.23$ Hz. $Q_1 = 12,689$ and $Q_2 = 13,771$ were calculated based on the relation $Q = f_0/\Delta f_0$. A difference of ~ 2.42 Hz between f_1 and f_2 was measured.

Since the $2f$ QEPAS C₂H₂ signal S_1 is affected by the modulation amplitude, this value has to be optimized. The $2f$ signal peak value as a function of laser modulation depth was measured by keeping fixed the laser emission wavelength at 1530.37 nm, modulating its current at $f_1/2$, while demodulating the QTF electrical signal at f_1 . The S_1 peak signal as a function of the modulation depth is shown in Fig. 3. The maximum value was obtained for a modulation depth of 13.8 mA, which was the value used in all the following experiments.

The $2f$ signals measured when only the QEPAS module (S_1) or the LITES module (S_2) were considered was retrieved using modulation frequencies of $f_1/2$ and $f_2/2$, respectively. Constant $f_1/2$ as the modulation frequency, the signal for system (S_3) would increase with the decrease of $|f_2 - f_1|$ and achieve the maximum when $|f_2 - f_1| = 0$. Therefore, $f_1/2$ was adopted as the system modulation frequency to show the superposition effect for system. As shown in Fig. 4, peak signals of 28.18 μ V, 69.76 μ V and 53.54 μ V were measured for S_1 , S_2 and S_3 , respectively, when operating at a temperature of 25.0 °C and a pressure of 750 Torr. The superposition effect evaluated by a coefficient η was measured considering the S_1 , S_2 and S_3 peak values and η is defined in percent as:

$$\eta = [S_3/(S_1 + S_2)] \times 100\% \quad (2)$$

In the ideal case of perfect frequency matching $\eta = 100\%$, while from the data of Fig. 4, η results only $\sim 54.7\%$, due to resonance frequency mismatching.

To explain the above result of poor η , a theoretical model was

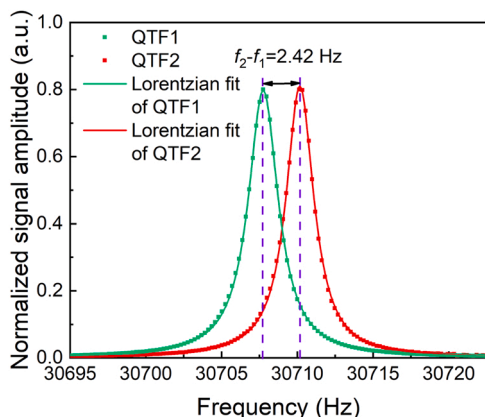


Fig. 2. Peak-normalized Lorentzian fit of frequency responses for QTFs.

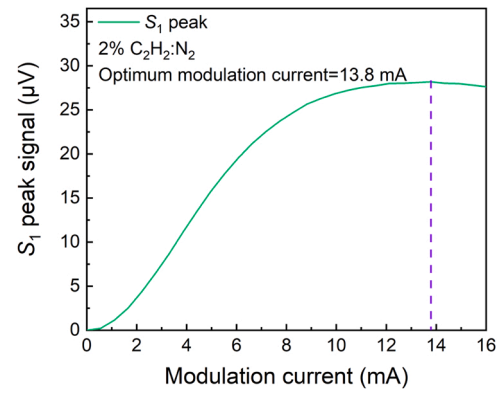


Fig. 3. S_1 peak signal as a function of the modulation current.

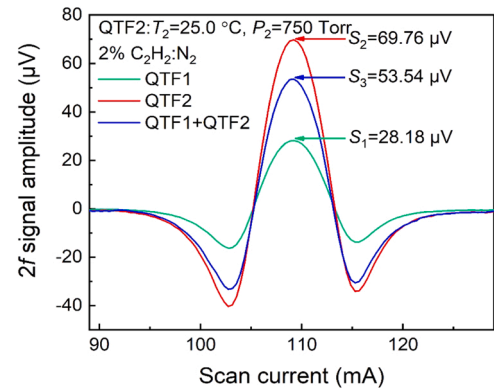


Fig. 4. S_1 , S_2 and S_3 spectral scans of the C₂H₂ absorption at 25.0 °C and atmospheric pressure.

presented. Due to the resonance characteristics of QTF, when the modulation frequency f deviates from half of the resonance frequency ($f_0/2$), the attenuation in Lorentzian form for QEPAS or LITES signal generated by QTF occurs. The maximum signal would be obtained when resonance frequency $f_0 = 2f$. This attenuation can be expressed as:

$$S \left(f, f_0, \Delta f_0 \right) = S \frac{1}{1 + \left(\frac{f - f_0/2}{\Delta f_0/2} \right)^2} \quad (3)$$

where $S(f, f_0, \Delta f_0)$ is the peak value of $2f$ QEPAS or LITES signal generated by QTF with a resonance frequency of f_0 and a bandwidth of Δf_0 in modulation frequency f , S is the peak value of the maximum $2f$ signal generated by QTF when $f = f_0/2$. Therefore, the peak value of system signal (S_3) can be expressed as:

$$S_3(f, f_1, f_2) = S_1 \frac{1}{1 + \left(\frac{f - f_1/2}{\Delta f_1/2} \right)^2} + S_2 \frac{1}{1 + \left(\frac{f - f_2/2}{\Delta f_2/2} \right)^2} \quad (4)$$

where S_1 is the peak value of the maximum $2f$ QEPAS signal generated by QTF1 when $f = f_1/2$, S_2 is the peak value of the maximum $2f$ LITES signal generated by QTF2 when $f = f_2/2$, $S_3(f, f_1, f_2)$ is the peak value of system signal in modulation frequency f . According to formula 4, for QTFs without frequency matching, the generated signals can hardly reach the maximum value S_1 and S_2 in modulation frequency f , the system signal will be far from the ideal value as a result. A simple simulation based on this formula was carried out through the substitution of S_1 , S_2 , f_1 , f_2 , Δf_1 , Δf_2 . When $f = f_1/2$, S_3 peak of 60.21 μ V and η of 61.5% were calculated, which were close to the experimental result.

3.2. Resonance frequency matching based on temperature regulation

In this section, QTF1 and QTF2 were the QTFs which had been used in Section 3.1. The QTF with resonance frequency of 30,707.75 Hz was QTF1 for QEPAS module and another QTF with resonance frequency of 30,710.17 Hz was QTF2 for LITES module. The performances of QTFs remained unchanged that peak $2f$ QEPAS signal for QTF1 (S_1) was 28.18 μV and peak $2f$ LITES signal for QTF2 (S_2) was 69.76 μV .

The operating temperature T_2 of QTF2 was regulated to tune its resonance frequency. The relationships between f_2 , Q_2 with T_2 were measured by optical excitation method and the obtained results are shown in Fig. 5. When T_2 increased from 25.0 $^{\circ}\text{C}$ to 35.0 $^{\circ}\text{C}$, f_2 also increased from 30,710.17 Hz to 30,710.49 Hz. While, at larger T_2 , f_2 decreased, down to a value of 30,706.77 Hz at $T_2 = 70.0$ $^{\circ}\text{C}$. The frequency matching $f_2 = f_1$ was achieved at $T_2 = 67.5$ $^{\circ}\text{C}$. Q_2 generally showed a downward trend from 13771 to 11373 with the increase of T_2 due to the increased energy dissipation. At the temperature of 67.5 $^{\circ}\text{C}$, $Q_2 = 12137$.

To test the efficacy of the frequency matching based on temperature regulation, we performed a series of C_2H_2 detection measurements while varying T_2 . The laser modulation frequency was set at $f_1/2$ when operating only with the QEPAS module or for the QEPAS+LITES measurements, while if only the LITES module was operated a modulation frequencies $f_2/2$ was used. Increasing T_2 , due to the minor change of Q_2 , the S_2 peak value remained almost unchanged. The relationship between the S_3 peak value and T_2 is shown in Fig. 6. Increasing T_2 , a minimum S_3 value of 42.31 μV was measured at 35.0 $^{\circ}\text{C}$, while the maximum S_3 value of 93.04 μV was achieved at 67.5 $^{\circ}\text{C}$. Indeed, the frequency difference between the QTFs reached its highest value at $T_2 = 35.0$ $^{\circ}\text{C}$, resulting in a poor superposition effect. When T_2 increased from 35.0 $^{\circ}\text{C}$ to 67.5 $^{\circ}\text{C}$, the frequency difference between QTFs was gradually reduced, reaching a good matching. Consequently, S_3 increased achieving a maximum value of 93.04 μV . When T_2 further rose to 70.0 $^{\circ}\text{C}$, the frequency difference increased and S_3 dropped to 85.87 μV .

At the optimal $T_2 = 67.5$ $^{\circ}\text{C}$ value and modulation frequency $f_1/2 = f_2/2 = 15353.87$ Hz, the measured $2f$ spectral scan for the QEPAS-LITES system (S_3) is shown in Fig. 7 and compared with the corresponding S_1 and S_2 spectra. Being the signals peak values $S_1 = 28.18$ μV , $S_2 = 69.76$ μV and $S_3 = 93.04$ μV , the superposition coefficient η for QEPAS-LITES system resulted $\sim 95.0\%$, significantly improved if compared with the 54.7% value measured without frequency matching. However, for a perfect matching S_3 should be 97.94 μV , i.e., $S_1 + S_2$, a value higher than the measured one. This slight difference is correlated to two main effects: a) loss of signals when superimposed by the adder; b) phase difference between QEPAS and LITES signals.

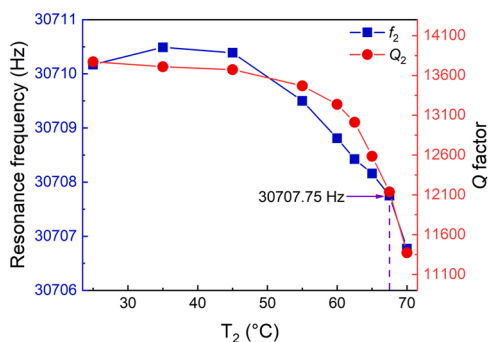


Fig. 5. Resonance frequency f_2 and quality factor Q_2 of QTF2 as a function of T_2 . The frequency matching between the two QTFs $f_2 = f_1 = 30,707.75$ Hz was achieved when $T_2 = 67.5$ $^{\circ}\text{C}$.

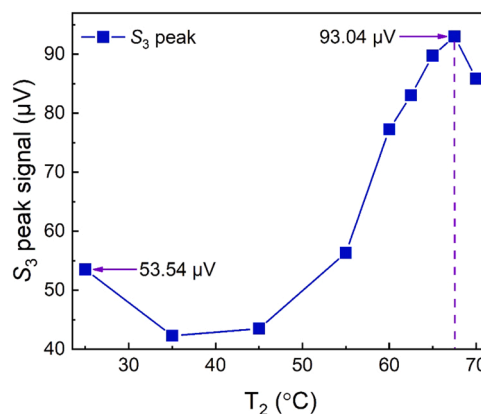


Fig. 6. S_3 peak signal as a function of T_2 . The maximum value of 93.04 μV was measured for $T_2 = 67.5$ $^{\circ}\text{C}$.

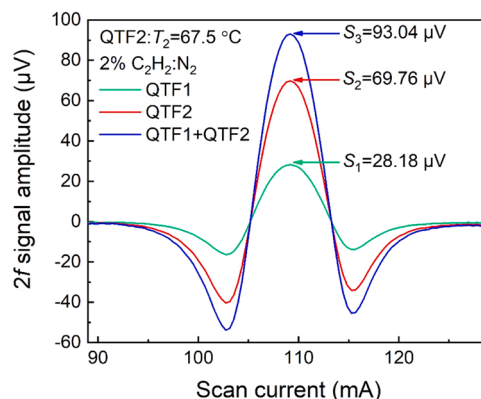


Fig. 7. $2f$ spectral scans measured at $T_2 = 67.5$ $^{\circ}\text{C}$ and a modulation frequency $f_1/2 = f_2/2 = 15,353.87$ Hz.

3.3. Resonance frequency matching based on pressure regulation

In this section, QTF1 and QTF2 were the QTFs which had been used in Section 3.1. However, due to the characteristic that QTF resonance frequency increases with the decrease of pressure, QTFs were interchanged compared to Section 3.1. The QTF with higher resonance frequency of 30,710.17 Hz was QTF1 for QEPAS module and another QTF with lower resonance frequency of 30,707.75 Hz was QTF2 for LITES module. The same as Section 3.1, peak $2f$ QEPAS signal for QTF1 (S_1) was 28.18 μV and peak $2f$ LITES signal for QTF2 (S_2) was 69.76 μV .

For these experiments, the temperature of the system was kept at 25.0 $^{\circ}\text{C}$, while the pressure P_2 for QTF2 was regulated to tune its resonance frequency and hence to achieve a frequency matching with QTF1. The relationship between f_2 , Q_2 with P_2 were measured by optical excitation method and the results are shown in Fig. 8. When P_2 decreased from 750 Torr to 475 Torr, f_2 increased from 30,707.75 Hz to 30,710.49 Hz. At 500 Torr, a frequency matched condition was achieved ($f_2 = f_1 = 30,710.17$ Hz). As expected, Q_2 showed an upward trend from 12,689 to 21,327 with the decrease of P_2 . At pressure of 500 Torr, $Q_2 = 19,686$.

Once again, we performed a series of C_2H_2 sensing while varying P_2 and modulated the laser at $f_1/2$ when operating only with the QEPAS module or for the QEPAS+LITES measurements, while at $f_2/2$ if only the LITES module is operated, as already described in Section 3.2. The relationship between S_2 and S_3 peak values with P_2 is shown in Fig. 9. When P_2 decreased from 750 Torr to 475 Torr, S_2 peak increased from 69.76 μV to 87.91 μV due to the related increase of Q_2 . At $P_2 = 500$ Torr, QTF1 and QTF2 were in frequency matching, and S_3 peak reached its

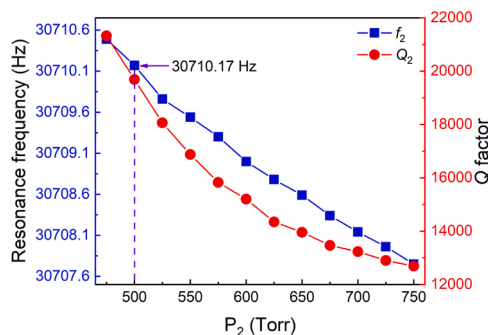


Fig. 8. Resonance frequency f_2 and quality factor Q_2 of QTF2 as a function of P_2 .

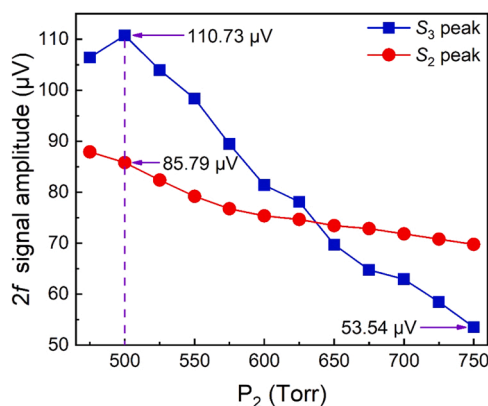


Fig. 9. S_2 and S_3 peak signal as a function of P_2 . The maximum value of $110.73 \mu\text{V}$ for S_3 was measured at $P_2 = 500$ Torr.

maximum value of $110.73 \mu\text{V}$.

At the optimal P_2 of 500 Torr value and modulation frequency $f_1/2 = f_2/2 = 15,355.08$ Hz, the measured S_3 spectral scan is shown in Fig. 10 and compared with the corresponding S_1 and S_2 spectra.

The peak values resulted $S_1 = 28.18 \mu\text{V}$, $S_2 = 85.79 \mu\text{V}$ and $S_3 = 110.73 \mu\text{V}$. Also in this case, S_3 resulted lower than the $(S_1 + S_2) = 113.97 \mu\text{V}$, for the same motivations reported in Section 3.2. However, the superposition coefficient η for QEPAS-LITES system resulted $\sim 97.2\%$, even higher than the value measured for resonance frequency matching based on temperature regulation ($\sim 95.0\%$).

4. Conclusion

One way to improve the performance of QTF-based gas sensing systems is the employment of multiple QTFs and superimposition of their signals. However, resonance frequency mismatching between the QTFs leads to a reduction in performance. Here, we proposed two different methods to achieve QTFs frequency matching in a QEPAS-LITES sensing system, based on a temperature or a pressure regulation of one of the QTF. C_2H_2 with a concentration of 2% in N_2 was selected as the target gas and two QTFs with resonance frequency f_0 around 30.7 kHz (at atmospheric pressure) where employed in a QEPAS-LITES setup to validate the proposed methods. Without resonance frequency regulation, a superposition coefficient η of only 54.7% was determined, due to a resonance frequency mismatch of ~ 2.42 Hz. For the temperature regulation methods, the resonance frequency matching condition was achieved for QTF2 operating at a temperature of 67.5°C and η increased to 95.0%. In case of resonance frequency matching based on pressure regulation, QTF2 operated at a pressure of 500 Torr and η increased up to 97.2%. The obtained results demonstrated that the proposed two methods are effective in nearly fully recover the

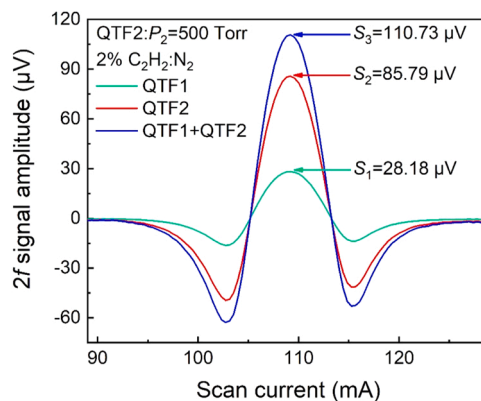


Fig. 10. $2f$ spectral scans measured at $P_2 = 500$ Torr and modulation frequency $f_1/2 = f_2/2 = 15,355.08$ Hz.

theoretical enhancement factor ($\eta = 100\%$). This is not only beneficial for multiple QTFs based laser spectroscopy sensing but can also be implemented for any QTF-based optical microscope and imaging sensing technique [40–43].

Declaration of Competing Interest

The authors declare that they have no known competing financial interests or personal relationships that could have appeared to influence the work reported in this paper.

Acknowledgments

We are grateful for financial supports from the National Natural Science Foundation of China (Grant No. 62022032, 61875047 and 61505041), Natural Science Foundation of Heilongjiang Province of China (Grant No. YQ2019F006), Fundamental Research Funds for the Central Universities, Financial Grant from the Heilongjiang Province Postdoctoral Foundation (Grant No. LBH-Q18052).

References

- [1] J.L. Bradshaw, J.D. Bruno, K.M. Lascola, R.P. Leavitt, J.T. Pham, F.J. Towner, D. M. Sonnenfroh, K.R. Parameswaran, Small, low-power consumption CO-sensor for post-fire cleanup aboard spacecraft, Proc. SPIE 8032 (2011) 80320D.
- [2] W. Ren, A. Farooq, D.F. Davidson, R.K. Hanson, CO concentration and temperature sensor for combustion gases using quantum-cascade laser absorption near $4.7 \mu\text{m}$, Appl. Phys. B 107 (3) (2012) 849–860.
- [3] T. Milde, M. Hoppe, H. Tatenguem, M. Mordmüller, J. Ogorman, U. Willer, W. Schade, J. Sacher, QEPAS sensor for breath analysis: a behavior of pressure, Appl. Opt. 57 (10) (2018) C120–C127.
- [4] Z. Wang, I. Cotton, S. Northcote, Dissolved gas analysis of alternative fluids for power transformers, IEEE Electr. Insul. Mag. 23 (2007) 5–14.
- [5] M.N. Baldin, S.M. Bobrovnikov, A.B. Vorozhtsov, E.V. Gorlov, V.M. Gruzov, V. I. Zharkov, Yu N. Panchenko, M.V. Pryamov, G.V. Sakovich, Effectiveness of combined laser and gas chromatographic remote detection of traces of explosives, Atmos. Ocean. Opt. 32 (2) (2019) 227–233.
- [6] K. Krzempek, G. Dudzik, K. Abramski, Photothermal spectroscopy of CO_2 in an intracavity mode-locked fiber laser configuration, Opt. Express 26 (2018) 28861–28871.
- [7] R. Rousseau, Z. Loghmani, M. Bahriz, K. Chamassi, R. Teissier, A.N. Baranov, A. Vicet, Off-beam QEPAS sensor using an $11\text{-}\mu\text{m}$ DFB-QCL with an optimized acoustic resonator, Opt. Express 27 (2019) 7435–7446.
- [8] Y.F. Ma, S.D. Qiao, Y. He, Y. Li, Z.H. Zhang, X. Yu, F.K. Tittel, Highly sensitive acetylene detection based on multi-pass retro-reflection-cavity-enhanced photoacoustic spectroscopy and a fiber amplified diode laser, Opt. Express 27 (10) (2019) 14163–14172.
- [9] A.A. Kosterev, Y.A. Bakhrirkin, R.F. Curl, F.K. Tittel, Quartz-enhanced photoacoustic spectroscopy, Opt. Lett. 27 (2002) 1902–1904.
- [10] A.G. Bell, On the production and reproduction of sound by light: the photophone, Am. J. Sci. 20 (1880) 305–324.
- [11] Y.F. Ma, Recent advances in QEPAS and QEPTS based trace gas sensing: a review, Front. Phys. 8 (2020) 268.
- [12] K. Liu, X.Y. Guo, H.M. Yi, W.D. Chen, W.J. Zhang, X.M. Gao, Off-beam quartz-enhanced photoacoustic spectroscopy, Opt. Lett. 34 (10) (2009) 1594–1596.

- [13] P. Patimisco, A. Sampaolo, L. Dong, M. Giglio, G. Scamarcio, F.K. Tittel, V. Spagnolo, Analysis of the electro-elastic properties of custom quartz tuning forks for optoacoustic gas sensing, *Sens. Actuators B* 227 (2016) 539–546.
- [14] H.D. Zheng, Y.H. Liu, H.Y. Lin, B. Liu, X.H. Gu, D.Q. Li, B.C. Huang, Y.C. Wu, L. P. Dong, W.G. Zhu, J.Y. Tang, H.Y. Guan, H.H. Lu, Y.C. Zhong, J.B. Fang, Y.H. Luo, J. Zhang, J.H. Yu, Z. Chen, F.K. Tittel, Quartz-enhanced photoacoustic spectroscopy employing pilot line manufactured custom tuning forks, *Photoacoustics* 17 (2020), 100158.
- [15] Y.F. Ma, S.D. Qiao, P. Patimisco, A. Sampaolo, Y. Wang, F.K. Tittel, V. Spagnolo, In plane quartz-enhanced photoacoustic spectroscopy, *Appl. Phys. Lett.* 116 (6) (2020), 061101.
- [16] P. Patimisco, A. Sampaolo, L. Dong, F.K. Tittel, V. Spagnolo, Recent advances in quartz enhanced photoacoustic sensing, *Appl. Phys. Rev.* 5 (1) (2018), 011106.
- [17] Q. Wang, Z. Wang, W. Ren, P. Patimisco, A. Sampaolo, V. Spagnolo, Fiber-ring laser intracavity QEPAS gas sensor using a 7.2 kHz quartz tuning fork, *Sens. Actuators B* 268 (2018) 512–518.
- [18] Y.F. Ma, R. Lewicki, M. Razeghi, F.K. Tittel, QEPAS based ppb-level detection of CO and N₂O using a high power CW DFB-QCL, *Opt. Express* 21 (1) (2013) 1008–1019.
- [19] J.P. Waclawek, H. Moser, B. Lendl, Compact quantum cascade laser based quartz-enhanced photoacoustic spectroscopy sensor system for detection of carbon disulfide, *Opt. Express* 24 (2016) 6559–6571.
- [20] M. Giglio, P. Patimisco, A. Sampaolo, A. Zifarelli, R. Blanchard, C. Pfluegl, M. F. Witinski, D. Vakhshoori, F.K. Tittel, V. Spagnolo, Nitrous oxide quartz-enhanced photoacoustic detection employing a broadband distributed-feedback quantum cascade laser array, *Appl. Phys. Lett.* 113 (2018), 171101.
- [21] Y.F. Ma, Y. Tong, Y. He, X.G. Jin, F.K. Tittel, Compact and sensitive mid-infrared all-fiber quartz-enhanced photo-acoustic spectroscopy sensor for carbon monoxide detection, *Opt. Express* 27 (6) (2019) 9302–9312.
- [22] Y.F. Ma, Y.H. Hong, S.D. Qiao, Z.T. Lang, X.N. Liu, H-shaped acoustic micro-resonator based quartz-enhanced photoacoustic spectroscopy, *Opt. Lett.* (2022), <https://doi.org/10.1364/OL.449822>.
- [23] Y.F. Ma, Y. He, Y. Tong, X. Yu, F.K. Tittel, Quartz-tuning-fork enhanced photothermal spectroscopy for ultra-high sensitive trace gas detection, *Opt. Express* 26 (24) (2018) 32103–32110.
- [24] X.N. Liu, S.D. Qiao, Y.F. Ma, Highly sensitive methane detection based on light-induced thermoelastic spectroscopy with a 2.33 μm diode laser and adaptive Savitzky-Golay filtering, *Opt. Express* 30 (2) (2022) 1304–1313.
- [25] Y. He, Y.F. Ma, Y. Tong, X. Yu, F.K. Tittel, Ultra-high sensitive light-induced thermoelastic spectroscopy sensor with a high Q-factor quartz tuning fork and a multipass cell, *Opt. Lett.* 44 (8) (2019) 1904–1907.
- [26] L. Hu, C.T. Zheng, M.H. Zhang, K.Y. Zheng, J. Zheng, Z. Song, X. Li, Y. Zhang, Y. D. Wang, F.K. Tittel, Long-distance in-situ methane detection using near-infrared light-induced thermo-elastic spectroscopy, *Photoacoustics* 21 (2021), 100230.
- [27] Y.F. Ma, Y. He, P. Patimisco, A. Sampaolo, S.D. Qiao, X. Yu, F.K. Tittel, V. Spagnolo, Ultra-high sensitive trace gas detection based on light-induced thermoelastic spectroscopy and a custom quartz tuning fork, *Appl. Phys. Lett.* 116 (1) (2020), 011103.
- [28] S.D. Qiao, Y. He, Y.F. Ma, Trace gas sensing based on single-quartz-enhanced photoacoustic-photothermal dual spectroscopy, *Opt. Lett.* 46 (10) (2021) 2449–2452.
- [29] S.D. Qiao, Y.F. Ma, Y. He, P. Patimisco, A. Sampaolo, V. Spagnolo, Ppt level carbon monoxide detection based on light-induced thermoelastic spectroscopy exploring custom quartz tuning forks and a mid-infrared QCL, *Opt. Express* 29 (16) (2021) 25100–25108.
- [30] S. Dello Russo, A. Zifarelli, P. Patimisco, A. Sampaolo, T.T. Wei, H.P. Wu, L. Dong, V. Spagnolo, Light-induced thermo-elastic effect in quartz tuning forks exploited as a photodetector in gas absorption spectroscopy, *Opt. Express* 28 (13) (2020) 19074–19084.
- [31] Z.T. Lang, S.D. Qiao, Y. He, Y.F. Ma, Quartz tuning fork-based demodulation of an acoustic signal induced by photo-thermo-elastic energy conversion, *Photoacoustics* 22 (2021), 100272.
- [32] C.G. Lou, H.J. Chen, X.T. Li, X. Yang, Y. Zhang, J.Q. Yao, Y.F. Ma, C. Chang, X. L. Liu, Graphene oxide and polydimethylsiloxane coated quartz tuning fork for improved sensitive near-and mid-infrared detection, *Opt. Express* 29 (13) (2021) 20190–20204.
- [33] T. Wei, A. Zifarelli, S. Dello Russo, H. Wu, G. Menduni, P. Patimisco, A. Sampaolo, V. Spagnolo, L. Dong, High and flat spectral responsivity of quartz tuning fork used as infrared photodetector in tunable diode laser spectroscopy, *Appl. Phys. Rev.* 8 (2021), 041409.
- [34] Y.F. Ma, X. Yu, G. Yu, X.D. Li, J.B. Zhang, D.Y. Chen, R. Sun, F.K. Tittel, Multi-quartz-enhanced photoacoustic spectroscopy, *Appl. Phys. Lett.* 107 (2) (2015), 021106.
- [35] Y.F. Ma, Y.Q. Hu, S.D. Qiao, F.K. Tittel, Trace gas sensing based on multi-quartz-enhanced photothermal spectroscopy, *Photoacoustics* 20 (2020), 100206.
- [36] Y.Q. Hu, S.D. Qiao, Y. He, Z.T. Lang, Y.F. Ma, Quartz-enhanced photoacoustic-photothermal spectroscopy for trace gas sensing, *Opt. Express* 29 (4) (2021) 5121–5127.
- [37] M. Christen, Air and gas damping of quartz tuning forks, *Sens. Actuators* 4 (1983) 555–564.
- [38] X.Y. Chen, X.C. Feng, X.J. Liu, X.Q. Zeng, Y. Xu, Low-cost quartz tuning fork based methane sensor for coal mine safety applications, *Sens. Actuators B* 295 (2019) 7–11.
- [39] Y.F. Ma, Y. He, L.G. Zhang, X. Yu, J.B. Zhang, R. Sun, F.K. Tittel, Ultra-high sensitive acetylene detection using quartz-enhanced photoacoustic spectroscopy with a fiber amplified diode laser and a 30.72 kHz quartz tuning fork, *Appl. Phys. Lett.* 110 (3) (2017), 031107.

- [40] D. Eliyahu, E. Gileadi, E. Galun, N. Eliaz, Atomic force microscope-based meniscus-confined three-dimensional electrodeposition, *Adv. Mater. Technol.* 5 (2020) 1900827.
- [41] M. Barbic, L. Eliason, J. Ranshaw, Femto-Newton force sensitivity quartz tuning fork sensor, *Sens. Actuators A* 136 (2007) 564–566.
- [42] U.W. Paetzold, S. Lehnen, K. Bittkau, U. Rau, R. Carius, Nanoscale observation of waveguide modes enhancing the efficiency of solar cells, *Nano Lett.* 14 (2014) 6599–6605.
- [43] R.D. Grober, J. Asimovic, J. Schuck, D. Hessman, P.J. Kindlemann, J. Hespanha, S. Morse, K. Karrai, I. Tiemann, S. Manus, Fundamental limits to force detection using quartz tuning forks, *Rev. Sci. Instrum.* 71 (2000) 2776.



Yufei Ma received his Ph.D. degree in physical electronics from Harbin Institute of Technology, China, in 2013. From September 2010 to September 2011, he spent as a visiting scholar at Rice University, USA. Currently, he is a professor at Harbin Institute of Technology, China. He is the winner of National Outstanding Youth Science Fund. His research interests include optical sensors, trace gas detection, laser spectroscopy, solid-state laser and optoelectronics. He has published more than 100 publications and given more than 20 invited presentations at international conferences. He serves as associate editor for *OSA Optics Express*, *SPIE Optical Engineering* and *Wiley Microwave and Optical Technology Letters*. He also serves as topical editor for *CLP Chinese Optics Letters* and editorial board member for Elsevier *Photoacoustics* and *MDPI Sensors*.



Yinqiu Hu received his B.S. degree in electronic science and technology from Harbin Institute of Technology, China, in 2020. He is now pursuing a M.S. degree of physical electronics from Harbin Institute of Technology. His research interest is light-induced thermoelastic spectroscopy based gas sensing.



Shunda Qiao received his B.S. degree in electronic science and technology from Yanshan university, China, in 2018. In 2020, he received his M.S. degree and began to pursue a PhD degree of physical electronics from Harbin institute of technology. His research interests include photoacoustic spectroscopy and its applications.



Ziting Lang received her B.S. degree in optoelectronic information science and engineering from Yanshan university, China, in 2020. She is now pursuing a PhD degree of physical electronics from Harbin Institute of Technology. Her research interest is photoacoustic spectroscopy based gas sensing.



Xiaonan Liu received her B.S. degree in automation from North China Electric Power University, China, in 2018, and received her M.S. degree in Power and Energy engineering from Harbin Engineering University, China, in 2021. Her is now pursuing a PhD degree of physical electronics from Harbin Institute of Technology. Her research interest is Combustion field diagnosis based on spectral measurement technology.



Ying He received his B.S. degree in optoelectronic material and device from Harbin Engineering University, China, in 2015, and received his M.S. degree in physical electronics from Harbin Institute of Technology China, in 2017. He is now pursuing a PhD degree of physical electronics from Harbin Institute of Technology. His research interests include photoacoustic spectroscopy and photothermal spectroscopy.



Vincenzo Spagnolo received the Ph.D., both in physics, from University of Bari in 1994. He works as Full Professor of Applied Physics at the Technical University of Bari. In 2019, he become Vice-president of the Technical University of Bari, deputy to Technology Transfer. The main scientific activity of Vincenzo Spagnolo has been related the development of opto-acoustic gas sensors based on quartz-enhanced photoacoustic spectroscopy. He has been visiting researcher at Rice University (Texas) in 2009 and 2010 and visiting professor in 2017. He is "hundred talents" visiting professor at Shanxi University in Taiyuan (China). Since 2017, he is the director of the joint-research lab PolySense, created by THORLABS GmbH and Technical University of Bari. His research activity is documented by more than 230 Scopus publications and three filed patents (more than 4500 citations, h-index 41). He has given more than 60 invited presentations at international conferences and workshops. Prof. Spagnolo is Fellow member of the SPIE and senior member of the Optica. Prof. Spagnolo has been ranked among Top 2% Scientists in the world by Stanford University, USA in both the career (<https://data.mendeley.com/datasets/btchxktzyw/1>) and the 2019 year list (<https://data.mendeley.com/datasets/btchxktzyw/2>).